

# Variational Autoencoder for Channel Estimation: Real-World Measurement Insights

Michael Baur, Benedikt Böck, Nurettin Turan, and Wolfgang Utschick

TUM School of Computation, Information and Technology, Technical University of Munich, Germany

Email: {mi.baur, benedikt.boeck, nurettin.turan, utschick}@tum.de

**Abstract**—This work utilizes a variational autoencoder for channel estimation and evaluates it on real-world measurements. The estimator is trained solely on noisy channel observations and parameterizes an approximation to the mean squared error-optimal estimator by learning observation-dependent conditional first and second moments. The proposed estimator significantly outperforms related state-of-the-art estimators on real-world measurements. We investigate the effect of pre-training with synthetic data and find that the proposed estimator exhibits comparable results to the related estimators if trained on synthetic data and evaluated on the measurement data. Furthermore, pre-training on synthetic data also helps to reduce the required measurement training dataset size.

**Index Terms**—Channel estimation, measurement data, deep neural network, generative model, variational autoencoder.

## I. INTRODUCTION

Model-based (MB) deep learning (DL) is an intriguing paradigm for the design of novel algorithms [1], which stands in opposition to end-to-end learning [2]. Instead of designing a task-specific deep neural network (DNN) whose aim is to learn most functionalities from scratch as most end-to-end approaches do, MB-DL utilizes established relationships and replaces only specific parts within the processing chain with a DNN. For instance, in channel estimation (CE), structural knowledge about a suboptimal approximation to the minimum mean squared error (MMSE) estimator is used for the blueprint of a convolutional neural network (CNN) [3] or a DNN serves as a denoiser for the LDAMP algorithm [4].

The recently proposed variational autoencoder (VAE)-based channel estimator is a MB-DL method for CE [5], [6], which can also be applied to estimation problems in time-varying and frequency-selective situations [7], [8]. The concept is to train a VAE on channel state information (CSI) data stemming from and representing a radio propagation environment to learn the underlying distribution. A remarkable property of the VAE is that it can be trained solely with noisy channel observations without access to perfect CSI during the training. Subsequently, the trained VAE is used to provide input data dependent conditional first and second moments to parameterize an approximation to the mean squared error (MSE)-optimal conditional mean estimator (CME). The VAE

This work is supported by the Bavarian Ministry of Economic Affairs, Regional Development and Energy within the project 6G Future Lab Bavaria. The authors acknowledge the financial support by the Federal Ministry of Education and Research of Germany in the program of “Souverän. Digital. Vernetzt.”. Joint project 6G-life, project identification number: 16KISK002

is a so-called generative model and was applied to a variety of other communications-related problems, e.g., channel equalization [9] or channel modeling [10]. Another prominent generative model representative is the generative adversarial network (GAN) [11]. Particularly, the GAN is applied to CE in hybrid, wideband, and quantized systems [12]–[14].

The VAE-based channel estimator from [6] demonstrates excellent CE results for realistic but, so far, synthetic channel data. Therefore, this work evaluates the VAE-based channel estimator on real-world measurement data, which was previously used to assess other data-driven estimators [15], [16]. The transition from synthetic to measured data is essential because many idealistic modeling assumptions in the synthetic case do not hold in reality. An example of such an idealistic assumption is array imperfections. We attain the following main insights from the evaluation with the measured data:

- The VAE-based estimator significantly outperforms the related estimators.
- For the best estimation quality, a large training dataset is necessary.
- A VAE trained on synthetic and evaluated on measured data shows comparable results as the best-performing related estimators.
- Pre-training with synthetic training data notably lowers the required measurement training dataset size.

## II. SYSTEM MODEL AND PROBLEM FORMULATION

We consider the uplink of a single-input multiple-output (SIMO) communications system with block-fading. The base station (BS) is equipped with a uniform rectangular array (URA) and has  $N_v$  antennas in its vertical and  $N_h$  antennas in its horizontal direction. Let  $N = N_v N_h$ . The mobile terminal (MT) is equipped with a single antenna. Under the assumption of a single-user scenario without pilot contamination, the BS receives a noisy pilot signal from the MT in the far field, which reads as

$$\mathbf{y} = \mathbf{h} + \mathbf{n}, \quad \mathbf{y} \in \mathbb{C}^N, \quad (1)$$

after decorrelating the single pilot. The frequency-flat assumed channel  $\mathbf{h}$  follows the unknown prior  $p(\mathbf{h})$  and is perturbed by additive white Gaussian noise (AWGN)  $\mathbf{n} \sim \mathcal{N}_{\mathbb{C}}(\mathbf{0}, \sigma^2 \mathbf{I})$ .

In the far field, the channel covariance matrix (CCM) of the channel entries in either vertical or horizontal direction is Toeplitz due to the uniform spacing at the URA. Consequently,

arXiv:2312.03450v2 [eess.SP] 8 Feb 2024

the CCM of all channel entries is block-Toeplitz. A block-Toeplitz structure can be enforced with the parameterization [17]:

$$\mathbf{Q}^H \text{diag}(\mathbf{c}) \mathbf{Q}, \quad \mathbf{c} \in \mathbb{R}_+^{4N}. \quad (2)$$

The matrix  $\mathbf{Q} = \mathbf{Q}_{N_v} \otimes \mathbf{Q}_{N_h}$ ,  $\mathbf{Q}_{N_v} \in \mathbb{C}^{2N_v \times 2N_v}$  contains the first  $N_v$  columns of the  $2N_v \times 2N_v$  discrete fourier transform (DFT) matrix, and  $\mathbf{Q}_{N_h}$  is defined accordingly.

In CE, the goal is to estimate  $\mathbf{h}$  based on  $\mathbf{y}$  from (1). The CME

$$\hat{\mathbf{h}}_{\text{CME}}(\mathbf{y}) = \mathbb{E}[\mathbf{h} | \mathbf{y}] = \arg \min_{\hat{\mathbf{h}} \in \mathbb{C}^N} \mathbb{E}[\|\mathbf{h} - \hat{\mathbf{h}}\|^2] \quad (3)$$

results in MSE-optimal channel estimates [18, Ch. 11]. By applying Bayes rule to  $p(\mathbf{h} | \mathbf{y})$  outcomes

$$p(\mathbf{h} | \mathbf{y}) = \frac{p(\mathbf{y} | \mathbf{h}) p(\mathbf{h})}{p(\mathbf{y})} = \frac{p_n(\mathbf{y} - \mathbf{A}\mathbf{h}) p(\mathbf{h})}{p(\mathbf{y})}, \quad (4)$$

which we utilize to reformulate the CME as

$$\mathbb{E}[\mathbf{h} | \mathbf{y}] = \int \mathbf{h} \frac{p_n(\mathbf{y} - \mathbf{A}\mathbf{h}) p(\mathbf{h})}{p(\mathbf{y})} d\mathbf{h}. \quad (5)$$

Note that  $p_n$  represents the distribution of  $\mathbf{n}$ . Eq. (5) reveals why the CME is hard to obtain in practice. It needs access to  $p(\mathbf{h})$ , i.e.,  $p(\mathbf{h})$  must be estimated directly or indirectly. Furthermore, the integral in (5) needs to be approximated since, in general, there exists no closed-form solution. The VAE is a generative model whose objective is the approximation of  $p(\mathbf{h})$ , and it provides a practical way to locally approximate the integral in (5). These properties motivate the application of the VAE to CE.

### III. VAE-BASED CHANNEL ESTIMATION

#### A. Preliminaries

The elaborations in this and the following section follow the description of the VAE-based channel estimator in [6], [8]. The evidence-lower bound (ELBO) is the central term for the training of a VAE and is a lower bound to a parameterized likelihood model  $p_\theta(\mathbf{y})$  of the unknown distribution  $p(\mathbf{y})$ . An accessible version of the ELBO reads as [19]

$$\mathcal{L}_{\theta, \phi}(\mathbf{y}) = \mathbb{E}_{q_\phi}[\log p_\theta(\mathbf{y} | \mathbf{z})] - \text{D}_{\text{KL}}(q_\phi(\mathbf{z} | \mathbf{y}) \| p(\mathbf{z})) \quad (6)$$

with  $\mathbb{E}_{q_\phi(\mathbf{z} | \mathbf{y})}[\cdot] = \mathbb{E}_{q_\phi}[\cdot]$  as the expectation according to the variational distribution  $q_\phi(\mathbf{z} | \mathbf{y})$ , which is supposed to approximate  $p_\theta(\mathbf{z} | \mathbf{y})$ . Note that the parameterization of  $p_\theta(\mathbf{z} | \mathbf{y})$  is determined by the joint  $p_\theta(\mathbf{y}, \mathbf{z})$  whose parameterization is set by  $p_\theta(\mathbf{y} | \mathbf{z})$ . The latent vector  $\mathbf{z} \in \mathbb{R}^{N_L}$  is introduced in the VAE to tractably improve the expressiveness of the parameterized likelihood model. The last term in (6) is the Kullback-Leibler (KL) divergence

$$\text{D}_{\text{KL}}(q_\phi(\mathbf{z} | \mathbf{y}) \| p_\theta(\mathbf{z})) = \mathbb{E}_{q_\phi} \left[ \log \left( \frac{q_\phi(\mathbf{z} | \mathbf{y})}{p_\theta(\mathbf{z})} \right) \right]. \quad (7)$$

The VAE optimizes the ELBO with the help of DNNs and the reparameterization trick [20]. To this end, it is necessary to define the involved distributions, which we fulfill as follows:

$$\begin{aligned} p(\mathbf{z}) &= \mathcal{N}(\mathbf{0}, \mathbf{I}), \\ p_\theta(\mathbf{y} | \mathbf{z}) &= \mathcal{N}_{\mathbb{C}}(\boldsymbol{\mu}_\theta(\mathbf{z}), \tilde{\mathbf{C}}_\theta(\mathbf{z})), \\ q_\phi(\mathbf{z} | \mathbf{y}) &= \mathcal{N}(\boldsymbol{\mu}_\phi(\mathbf{y}), \text{diag}(\boldsymbol{\sigma}_\phi^2(\mathbf{y}))), \end{aligned} \quad (8)$$

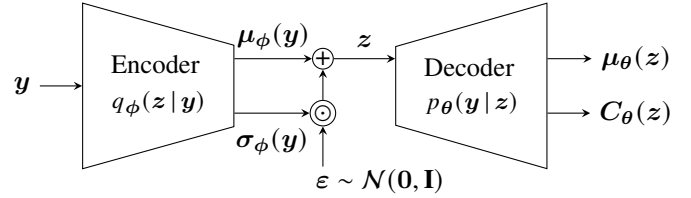


Fig. 1. Structure of a VAE with CG distributions  $q_\phi(\mathbf{z} | \mathbf{y})$  and  $p_\theta(\mathbf{y} | \mathbf{z})$ . The encoder and decoder represent DNNs.

and  $\tilde{\mathbf{C}}_\theta(\mathbf{z}) = \mathbf{C}_\theta(\mathbf{z}) + \zeta^2 \mathbf{I}$ . Both  $p_\theta(\mathbf{y} | \mathbf{z})$  and  $q_\phi(\mathbf{z} | \mathbf{y})$  are therefore conditionally Gaussian (CG) distributions, realized by DNNs with parameters  $\theta$  and  $\phi$ . Accordingly, we obtain closed-form expressions for the terms in (6), i.e.,  $(-\mathbb{E}_{q_\phi}[\log p_\theta(\mathbf{y} | \mathbf{z})])$  is replaced by the estimate

$$\log \det(\pi \tilde{\mathbf{C}}_\theta(\tilde{\mathbf{z}})) + (\mathbf{h} - \boldsymbol{\mu}_\theta(\tilde{\mathbf{z}}))^H \tilde{\mathbf{C}}_\theta^{-1}(\tilde{\mathbf{z}}) (\mathbf{h} - \boldsymbol{\mu}_\theta(\tilde{\mathbf{z}})) \quad (9)$$

with the single monte carlo sample  $\tilde{\mathbf{z}} \sim q_\phi(\mathbf{z} | \mathbf{y})$ . The term  $\text{D}_{\text{KL}}(q_\phi(\mathbf{z} | \mathbf{y}) \| p_\theta(\mathbf{z}))$  is the KL divergence between two Gaussian distributions, which becomes

$$\frac{1}{2} \left( \mathbf{1}^T \left( -\log \sigma_\phi^2(\mathbf{y}) + \boldsymbol{\mu}_\phi(\mathbf{y})^2 + \boldsymbol{\sigma}_\phi^2(\mathbf{y}) \right) - N_L \right), \quad (10)$$

where  $\mathbf{1}$  represents the all-ones vector. A schematic illustration of a VAE implementation is displayed in Fig. 1. The presented VAE consists of an encoder that represents  $q_\phi(\mathbf{z} | \mathbf{y})$  and outputs  $\{\boldsymbol{\mu}_\phi(\mathbf{y}), \boldsymbol{\sigma}_\phi(\mathbf{y})\}$  and a decoder that represents  $p_\theta(\mathbf{y} | \mathbf{z})$  and outputs  $\{\boldsymbol{\mu}_\theta(\mathbf{z}), \mathbf{C}_\theta(\mathbf{z})\}$ . The encoder receives  $\mathbf{y}$  as input and produces with its outputs the reparameterized sample  $\mathbf{z}$ , which is the decoder input. We refer the reader to [6], [19] for a more detailed introduction to the VAE framework.

#### B. MMSE Estimation with the VAE

After successfully training the VAE, we obtain a generative model that locally parameterizes  $p(\mathbf{y})$  as CG. For estimation purposes, it is indeed more desirable to have a parametric model for  $p(\mathbf{h})$ . We can achieve this for the system model in (1) by requiring the VAE decoder outputs  $\boldsymbol{\mu}_\theta(\mathbf{z})$  and  $\mathbf{C}_\theta(\mathbf{z})$  to be the mean and covariance of  $\mathbf{h} | \mathbf{z}$  instead of  $\mathbf{y} | \mathbf{z}$ . Since we have an AWGN channel, where knowledge of the noise variance is assumed, we add  $\zeta^2 \mathbf{I}$  to  $\mathbf{C}_\theta(\mathbf{z})$  for the computation of (9) during the training to acquire the intended outcome. It follows that the VAE's goal is to provide

$$\mathbf{h} | \mathbf{z} \sim p_\theta(\mathbf{h} | \mathbf{z}) = \mathcal{N}_{\mathbb{C}}(\boldsymbol{\mu}_\theta(\mathbf{z}), \mathbf{C}_\theta(\mathbf{z})) \quad (11)$$

after the training. The VAE learns abstract conditions  $\mathbf{z}$  in its latent space that may not necessarily carry a physical interpretation. The advantage of the abstractness of the condition is the flexibility to model the channels as CG since the model can select an almost arbitrary condition for every channel. The CG property will be central for the design of the channel estimator.

Section II describes that the CME delivers MMSE channel estimates. The CME can be reformulated with the law of total expectation as

$$\mathbb{E}[\mathbf{h} | \mathbf{y}] = \mathbb{E}_{p_\theta(\mathbf{z} | \mathbf{y})} [\mathbb{E}[\mathbf{h} | \mathbf{z}, \mathbf{y}] | \mathbf{y}]. \quad (12)$$

Further, let  $t_\theta(\mathbf{z}, \mathbf{y}) = \mathbb{E}[\mathbf{h} | \mathbf{z}, \mathbf{y}]$ . Assuming that (11) holds, a closed-form solution for  $t_\theta(\mathbf{z}, \mathbf{y})$  exists due to the CG property. Therefore [18, Ch. 11],

$$t_\theta(\mathbf{z}, \mathbf{y}) = \boldsymbol{\mu}_\theta(\mathbf{z}) + \mathbf{C}_\theta(\mathbf{z})(\mathbf{C}_\theta(\mathbf{z}) + \varsigma^2 \mathbf{I})^{-1}(\mathbf{y} - \boldsymbol{\mu}_\theta(\mathbf{z})), \quad (13)$$

with  $\mathbf{y}$  from (1). The latent vector  $\mathbf{z}$  depends on  $\mathbf{y}$  through the encoder. The quantities  $\boldsymbol{\mu}_\theta(\mathbf{z})$  and  $\mathbf{C}_\theta(\mathbf{z})$  are provided by the decoder of the VAE. It remains to compute the outer expectation in (12), with respect to  $p_\theta(\mathbf{z} | \mathbf{y})$ . Since  $p_\theta(\mathbf{z} | \mathbf{y})$  is approximated by  $q_\phi(\mathbf{z} | \mathbf{y})$ , we can approximate the outer expectation with samples from  $q_\phi(\mathbf{z} | \mathbf{y})$ . As analyzed in detail in [6], the single sample  $\boldsymbol{\mu}_\phi(\mathbf{z})$  from  $q_\phi(\mathbf{z} | \mathbf{y})$  achieves excellent CE performance. With all the previous depictions, we obtain the VAE-based estimator

$$\hat{\mathbf{h}}_{\text{VAE}}(\mathbf{y}) = t_\theta(\mathbf{z} = \boldsymbol{\mu}_\phi(\mathbf{y}), \mathbf{y}). \quad (14)$$

The estimator  $\hat{\mathbf{h}}_{\text{VAE}}(\mathbf{y})$  requires an offline training phase of the VAE in Fig. 1 to provide the necessary first and second conditional moment for the evaluation of  $t_\theta(\mathbf{z}, \mathbf{y})$ . An intriguing aspect of the estimator in this work is that its training is based solely on noisy observations  $\mathbf{y}$  and not on perfect CSI data  $\mathbf{h}$ . This contrasts the plethora of DL-based estimators, that usually require perfect CSI during the training, which is only available after measurement campaigns. We thus think that  $\hat{\mathbf{h}}_{\text{VAE}}(\mathbf{y})$  is a realistic estimator that matches real-world necessities. The estimator  $\hat{\mathbf{h}}_{\text{VAE}}(\mathbf{y})$  may also be extended to underdetermined systems, e.g., for hybrid and wideband systems [8]. However, the treatment of such cases exceeds the scope of this work. Previous work demonstrated that  $\hat{\mathbf{h}}_{\text{VAE}}(\mathbf{y})$  achieves excellent CE performance for the SIMO system model [5], [6], which we want to verify for real-world measurements in this work.

### C. Practical Considerations

For the evaluation of  $\hat{\mathbf{h}}_{\text{VAE}}(\mathbf{y})$ , the matrix  $\mathbf{C}_\theta(\mathbf{z})$  must approximate the true CCM as well as possible. Since we have a URA at the BS, we can exploit the resulting block-Toeplitz structure of the CCM in (2) for the parameterization of  $\mathbf{C}_\theta(\mathbf{z})$ . Straightforwardly, we propose to approximate the URA CCM in the VAE framework with

$$\mathbf{C}_\theta(\mathbf{z}) = \mathbf{Q}^H \text{diag}(\mathbf{c}_\theta(\mathbf{z})) \mathbf{Q}, \quad \mathbf{c}_\theta(\mathbf{z}) \in \mathbb{R}_+^{4N}, \quad (15)$$

where  $\mathbf{Q}$  is defined as in (2). The vector  $\mathbf{c}_\theta(\mathbf{z})$  is outputted by the VAE decoder.

The computational complexity of an estimator is an essential aspect for CE. The complexity of  $\hat{\mathbf{h}}_{\text{VAE}}(\mathbf{y})$  consists of two parts: a forward pass of the VAE to yield the decoder outputs and one evaluation of (13). For the VAE forward pass, we can utilize the analysis from [6], as the VAE architecture is conceptually the same. The complexity for the  $D$  layer VAE was found to be  $\mathcal{O}(DN^2)$ , which is a consequence of the final linear layer (LL) that yields the decoder outputs. This outcome also holds for the model in this work. The second part of the computational complexity relates to the evaluation of (13) and is dominated by the inversion of the matrix  $\mathbf{C}_\theta(\mathbf{z}) + \varsigma^2 \mathbf{I}$ . The inversion of this positive-definite block-Toeplitz matrix can be completed in  $\mathcal{O}(N^2)$  time with

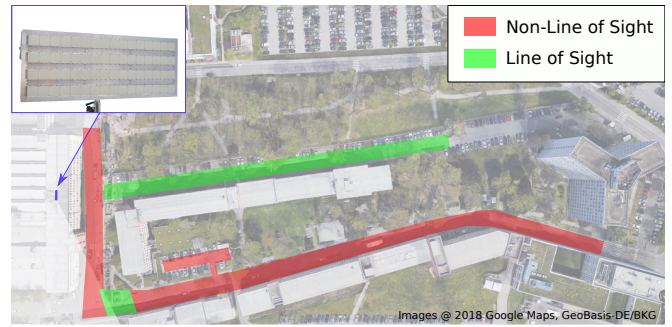


Fig. 2. Measurement setup on the Nokia campus in Stuttgart, Germany.

the Levinson algorithm [21, Ch. 6]. In conclusion, the worst-case complexity for the computation of  $\hat{\mathbf{h}}_{\text{VAE}}(\mathbf{y})$  is  $\mathcal{O}(DN^2)$ , which can be further reduced by parallel computations and network pruning of the DNN.

## IV. CSI DATA ACQUISITION

### A. Measurement Campaign

As described in [15], [16], the measurement campaign was conducted at the Nokia campus in Stuttgart, Germany, in 2017. Fig. 2 displays the scenario. On a rooftop roughly 20 m above the ground, the BS is located with a  $10^\circ$  down-tilt. The BS is a  $4 \times 16$  URA with horizontal single polarized patch antennas and was adapted to match the 3rd Generation Partnership Project (3GPP) Urban Microcell (UMi) propagation scenario. As a result,  $N_v = 4$  and  $N_h = 16$ . The antenna spacing is  $\lambda$  in the vertical and  $\lambda/2$  in the horizontal direction, with  $\lambda$  being the wavelength. The single monopole receive antenna representing the MT was placed on a moving vehicle with a maximum speed of 25 km/h. GPS was used for the synchronization between the transmitter and receiver. The data was collected by a TSMW receiver and stored on a Rohde & Schwarz IQR hard disk recorder. The carrier frequency was 2.18 GHz. The BS transmitted 10 MHz orthogonal frequency division multiplexing (OFDM) waveforms with 600 subcarriers in 15 kHz spacing. The pilots were sent continuously with a periodicity of 0.5 ms, arranged in 50 separate subbands, with 12 consecutive subcarriers each. The propagation channel was assumed to remain constant for one pilot burst.

Channel realization vectors with 64 coefficients per subband were extracted in a post-processing step. The measurement campaign was conducted at a high signal-to-noise ratio (SNR) between 20 and 30 dB. Such high SNRs are necessary to obtain almost perfect CSI data needed for the offline training of most DL-based channel estimators, e.g. [3], [22], [23]. We corrupt the measured channels with AWGN at specific SNR values to generate noisy observations according to (1). For the training of the VAE-based channel estimator presented in Section III-B, it is not required to actually conduct a measurement campaign at such high SNR values to obtain almost perfect CSI data. Instead, it would suffice to gather a dataset of noisy observations  $\mathbf{y}$  from (1) at SNR values that are present in the online estimation phase received and collected at the BS during regular operation.

## B. Synthetic Data

Besides measured data, we also need synthetic CSI data for the analysis in Section V. To this end, we utilize the QuaDRiGa channel simulator in version 2.6.1 to generate artificial channel vector realizations [24]. The channels are supposed to belong to a 3GPP UMi scenario, and the environment in QuaDRiGa is designed to approximate the measurement site in Fig. 2 as close as possible. This includes using the same carrier frequency of 2.18 GHz, placing the BS at a similar height and distance to the MTs, and assigning the MTs a comparable velocity. The BS is also equipped with a URA and comprises identical dimensions and spacings as in the measurement data. QuaDRiGa models the channels as a superposition of in total  $L$  propagation paths, where  $L$  is determined whether line of sight (LOS) or non-line of sight (NLOS) conditions are present. More precisely, a channel is given as  $\mathbf{h} = \sum_{\ell=1}^L \mathbf{g}_\ell \exp(-2\pi j f_c \tau_\ell)$ , with  $f_c$  as the carrier frequency and  $\tau_\ell$  as the delay of the  $\ell$ -th propagation path. The vector  $\mathbf{g}_\ell$  accounts for the path attenuation between the MT and every receive antenna, the antenna radiation pattern, and the polarization. Eventually, the generated channels are post-processed to normalize the path gains.

## V. SIMULATION RESULTS

### A. Implementation Details

For the measurement data, we obtain a dataset of size 420,000 of which we use  $T_r = 400,000$  samples for training,  $T_v = 10,000$  for validation, and  $T_e = 10,000$  for testing. For the synthetic QuaDRiGa data, we generate in total 520,000 channels, which are split into 500,000, 10,000, and 10,000 training, validation, and test samples, respectively. The channels are normalized in each dataset such that  $E[\|\mathbf{h}\|^2] = N$ . Accordingly, we define the SNR as  $1/\varsigma^2$ . We evaluate our methods with the normalized mean squared error (NMSE)

$$\text{NMSE} = \frac{1}{T_e N} \sum_{i=1}^{T_e} \|\mathbf{h}_i - \hat{\mathbf{h}}_i\|^2, \quad (16)$$

where  $\mathbf{h}_i$  is the  $i$ -th channel realization in the test dataset, and  $\hat{\mathbf{h}}_i$  the corresponding estimate.

Conceptually, the VAE architecture is identical to the one presented in [6]. The real and imaginary parts of  $\mathbf{y}$  are stacked as convolutional channels (CCs) and serve as VAE encoder input. A  $1 \times 1$  convolutional layer (CL) follows that maps to CH CCs to which we refer in Table I. Three building blocks consisting of a CL, a batch normalization (BN), and a ReLU activation function follow, where the CC number is multiplied by 1.75 and rounded after each CL. A subsequent LL maps the flattened vector to the encoder outputs  $\{\mu_\phi(\mathbf{y}), \sigma_\phi(\mathbf{y})\}$ . The decoder is a symmetrically flipped version of the encoder, which implies that all CLs are replaced with transposed CLs. The remaining layer types remain unchanged. The final transposed CL maps to three CLs. A flattening follows and a final LL maps to  $\{\mu_\theta(\mathbf{z}), c_\theta(\mathbf{z})\}$ . We enforce strictly positive values in  $\sigma_\phi(\mathbf{y})$  and  $c_\theta(\mathbf{z})$  with an exponential function. In all CLs, we use 1D CLs with a kernel size of eleven and a stride of two. For the optimization, we use Adam as optimizer with

TABLE I  
PERFORMANCE OF VAES WITH INCREASING PARAMETER AMOUNT.

VAE	CH	parameters	NMSE at 10 dB	NMSE at 20 dB
1	4	319,291	$3.574 \cdot 10^{-2}$	$6.288 \cdot 10^{-3}$
2	16	449,973	<b><math>3.346 \cdot 10^{-2}</math></b>	<b><math>6.149 \cdot 10^{-3}</math></b>
3	32	698,353	$3.350 \cdot 10^{-2}$	$6.279 \cdot 10^{-3}$
4	64	1,452,249	$3.363 \cdot 10^{-2}$	$6.271 \cdot 10^{-3}$

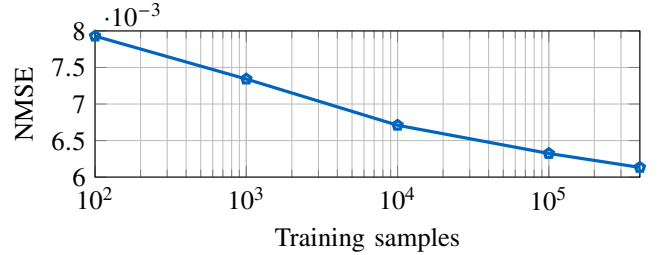


Fig. 3. NMSE for different numbers of training samples at an SNR of 20 dB for the measurement data channels.

a learning rate of  $5 \cdot 10^{-4}$  and a batch size of 256. The latent space dimensionality  $N_L$  is 32. The implementation is realized with *PyTorch*. Unless stated otherwise, we train each VAE until it does not improve in terms of NMSE on the validation dataset for 100 consecutive epochs.

### B. Architecture Study

As pointed out in the previous subsection, the encoder input is mapped to CH CLs, which is multiplied by 1.75 after each following CL. Since CH controls the number of parameters in the VAE, we want to investigate the relation between the number of parameters and the estimation performance by varying CH. To this end, we display different model sizes and their performance at 10 and 20 dB on the measurement test dataset in Table I. We observe that the second model achieves the lowest NMSE at both SNR values. Hence, making CH larger than 16 does not improve the performance, so we utilize this value for CH in the remainder of this work.

To determine whether the full measurement training dataset achieves convergence of the model parameters, we illustrate the NMSE at 20 dB on the measurement test dataset for the VAE estimator with different sizes of the training dataset, ranging from 100 to 400,000 in Fig. 3. As can be seen, the most significant performance gain is achieved until 100,000 training samples are considered. When 400,000 are considered, the NMSE still improves by a small value. Fig. 3 highlights that a large training dataset is required for the considered model size to reach the full estimation potential.

### C. Estimation Results

We investigate the estimation performance in terms of NMSE on the measurement test dataset of the proposed VAE-based estimator in Fig. 4. The word in brackets tells the dataset used for training the VAE, i.e., the blue curve belongs to the measurement training dataset and the green curve to the QuaDRiGa training dataset. The latter means that the VAE did

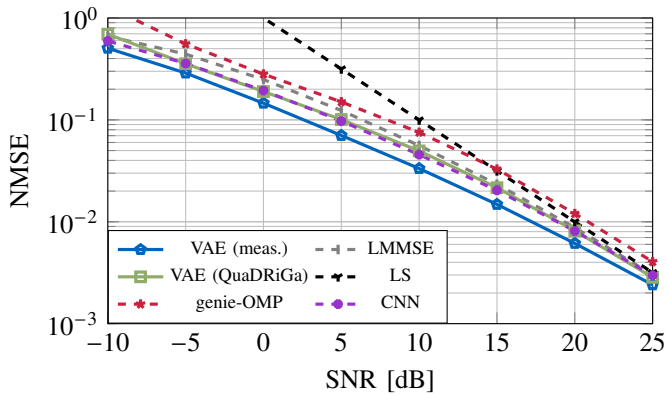


Fig. 4. Evaluation of the NMSE for the measurement test dataset. The proposed methods are displayed with solid linestyles.

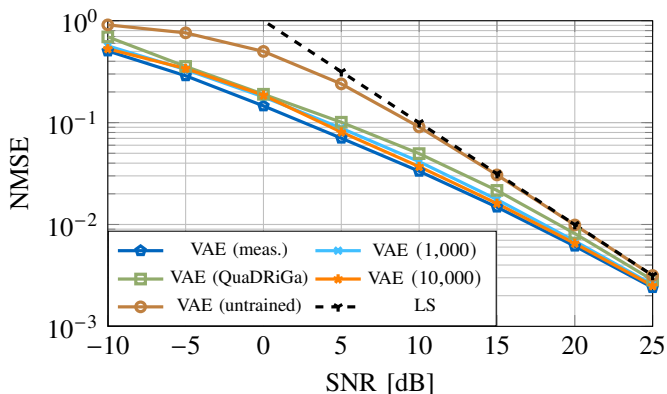


Fig. 5. Evaluation of the NMSE for the measurement test dataset, which were pre-trained on QuaDRiGa channel data.

not see any measurement dataset sample during its training. As related baseline estimators, we display:

- LMMSE: computes a global sample covariance matrix from the measurement training dataset and a linear minimum mean squared error (LMMSE) estimate as in [6]
- LS: a least squares (LS) estimate
- CNN: a CNN-based estimator [3]
- genie-OMP: the orthogonal matching pursuit (OMP) algorithm that uses a four-times oversampled block-circulant matrix as a dictionary [25]

In Fig. 4, it is visible that VAE (meas.) clearly outperforms all other methods at all SNR values. Remarkably, VAE (QuaDRiGa) performs almost identically as CNN, and both methods are the second best-performing estimators, followed by LMMSE. A possible explanation for the fair performance of VAE (QuaDRiGa) is that QuaDRiGa generates propagation scenarios that resemble the measurement scenario. Supposedly, the result is that both channel distributions are alike, which is beneficial for the online estimation phase.

It is desirable to reduce the necessary training data of real-world measurements as much as possible. One conceivable way is to pre-train the model on synthetic data and do the actual training on a smaller dataset. We do this in Fig. 5 by pre-training VAEs on the QuaDRiGa training dataset. The number

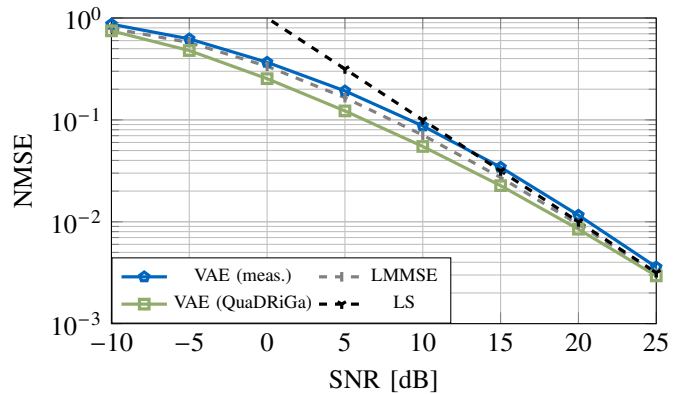


Fig. 6. Evaluation of the NMSE for the QuaDRiGa test dataset.

in brackets is the number of training samples we use from the measurement data. The blue and green curves represent the same models as in Fig. 4. Fig. 5 shows that using a small number of measurement training data after pre-training with QuaDRiGa data further improves the NMSE. Compared with Fig. 3, where no pre-training with QuaDRiGa was performed, the relative performance gain with 1,000 and 10,000 measurement training samples is 6.3% and 2.8%. Thus, the gain with fewer samples is more noticeable. We also plot a VAE with untrained weights only randomly initialized. This produces an identity matrix as estimated CCM for every channel, which results in the NMSE  $1/(SNR+1)$ . The explanation for this behavior is that we use an exponential function to enforce positive values in the vector  $c_{\theta}(z)$ , which receives only zeros as input due to the random weights.

At last, we want to cross-check the previous analysis by evaluating a VAE on QuaDRiGa data that is trained on the measurement data. This investigation is presented in Fig. 6. The plot shows a comparable performance gap between the two VAEs as in Fig. 4, but in Fig. 6 VAE (QuaDRiGa) obviously (must) perform better. Since VAE (meas.) performs worse than LS in the high SNR, it can be concluded that it is not advisable to transfer a model from the measurement to the QuaDRiGa data, which implies that the measurement data is more site-specific. However, the other direction appears reasonable based on the observations in Fig. 4 and 5.

## VI. CONCLUSION

This paper presents the evaluation of a VAE-based channel estimator on data stemming from real-world measurements. The VAE-based estimator shows superior channel estimation performance compared to related state-of-the-art estimators. A downside of the VAE-based method is its requirement for an extensive training dataset to develop its full estimation potential. Pre-training with synthetic channel data mitigates this necessity notably. However, since the VAE can be trained solely with noisy observations, the extensive training dataset requirement is not severe, as noisy observations can seamlessly be collected during regular BS operation until the desired training dataset size is achieved. Our future work includes the analysis of the VAE-based estimator in a real-world system.

## REFERENCES

- [1] N. Shlezinger, J. Whang, Y. C. Eldar, and A. G. Dimakis, "Model-Based Deep Learning," *Proc. IEEE*, vol. 111, no. 5, pp. 465–499, 2023.
- [2] W. Yu, F. Sotiriou, and T. Jiang, "Role of Deep Learning in Wireless Communications," *IEEE BITS Inf. Theory Mag.*, vol. 2, no. 2, pp. 56–72, 2022.
- [3] D. Neumann, T. Wiese, and W. Utschick, "Learning The MMSE Channel Estimator," *IEEE Trans. Signal Process.*, vol. 66, no. 11, pp. 2905–2917, 2018.
- [4] H. He, C. K. Wen, S. Jin, and G. Y. Li, "Deep Learning-Based Channel Estimation for BeamSpace mmWave Massive MIMO Systems," *IEEE Wirel. Commun. Lett.*, vol. 7, no. 5, pp. 852–855, 2018.
- [5] M. Baur, B. Fesl, M. Koller, and W. Utschick, "Variational Autoencoder Leveraged MMSE Channel Estimation," in *56th Asilomar Conf. Signals, Syst., Comput.* Pacific Grove, CA, USA: IEEE, 2022, pp. 527–532.
- [6] M. Baur, B. Fesl, and W. Utschick, "Leveraging Variational Autoencoders for Parameterized MMSE Channel Estimation," *arXiv preprint arXiv:2307.05352*, 2023.
- [7] B. Böck, M. Baur, V. Rizzello, and W. Utschick, "Variational Inference Aided Estimation of Time Varying Channels," in *2023 IEEE Int. Conf. Acoust. Speech Signal Process.* Rhodes Island, Greece: IEEE, 2023, pp. 1–5.
- [8] M. Baur, N. Turan, B. Fesl, and W. Utschick, "Channel Estimation in Underdetermined Systems Utilizing Variational Autoencoders," *arXiv preprint arXiv:2309.08411*, 2023.
- [9] V. Lauinger, F. Buchali, and L. Schmalen, "Blind Equalization and Channel Estimation in Coherent Optical Communications Using Variational Autoencoders," *IEEE J. Sel. Areas Commun.*, vol. 40, no. 9, pp. 2529–2539, 2022.
- [10] W. Xia, S. Rangan, M. Mezzavilla, A. Lozano, G. Geraci, V. Semkin, and G. Loiano, "Generative Neural Network Channel Modeling for Millimeter-Wave UAV Communication," *IEEE Trans. Wirel. Commun.*, vol. 21, no. 11, pp. 9417–9431, 2022.
- [11] I. Goodfellow, J. Pouget-Abadie, M. Mirza, B. Xu, D. Warde-Farley, S. Ozair, A. Courville, and Y. Bengio, "Generative Adversarial Networks," *Commun. ACM*, vol. 63, no. 11, pp. 139–144, 2020.
- [12] E. Balevi and J. G. Andrews, "Wideband Channel Estimation With a Generative Adversarial Network," *IEEE Trans. Wirel. Commun.*, vol. 20, no. 5, pp. 3049–3060, 2021.
- [13] A. S. Doshi, M. Gupta, and J. G. Andrews, "Over-the-Air Design of GAN Training for mmWave MIMO Channel Estimation," *IEEE J. Sel. Areas Inf. Theory*, vol. 3, no. 3, pp. 557–573, 2022.
- [14] A. Doshi and J. G. Andrews, "One-Bit mmWave MIMO Channel Estimation Using Deep Generative Networks," *IEEE Wirel. Commun. Lett.*, vol. 12, no. 9, pp. 1593–1597, 2023.
- [15] C. Hellings, A. Dehmani, S. Wesemann, M. Koller, and W. Utschick, "Evaluation of Neural-Network-Based Channel Estimators Using Measurement Data," in *23rd Int. ITG Work. Smart Antennas*, Vienna, Austria, 2019, pp. 164–168.
- [16] N. Turan, B. Fesl, M. Grundei, M. Koller, and W. Utschick, "Evaluation of a Gaussian Mixture Model-based Channel Estimator using Measurement Data," in *2022 Int. Symp. Wirel. Commun. Syst.* IEEE, 2022, pp. 1–6.
- [17] G. Strang, "A Proposal for Toeplitz Matrix Calculations," *Stud. Appl. Math.*, vol. 74, no. 2, pp. 171–176, 1986.
- [18] S. M. Kay, *Fundamentals of Statistical Signal Processing: Estimation Theory*. Englewood Cliffs, NJ: Prentice-Hall, Inc., 1993.
- [19] D. P. Kingma and M. Welling, "An Introduction to Variational Autoencoders," *Found. Trends® Mach. Learn.*, vol. 12, no. 4, pp. 307–392, 2019.
- [20] —, "Auto-Encoding Variational Bayes," in *Proc. 2nd Int. Conf. Learn. Represent.*, 2014.
- [21] S. M. Kay, *Modern Spectral Estimation: Theory and Application*. Englewood Cliffs, NJ: Prentice-Hall, Inc., 1988.
- [22] H. Ye, G. Y. Li, and B. H. Juang, "Power of Deep Learning for Channel Estimation and Signal Detection in OFDM Systems," *IEEE Wirel. Commun. Lett.*, vol. 7, no. 1, pp. 114–117, 2018.
- [23] M. Soltani, V. Pourahmadi, A. Mirzaei, and H. Sheikhzadeh, "Deep Learning-Based Channel Estimation," *IEEE Commun. Lett.*, vol. 23, no. 4, pp. 2019–2022, 2019.
- [24] S. Jaeckel, L. Raschkowski, K. Borner, and L. Thiele, "QuaDRiGa: A 3-D Multi-Cell Channel Model With Time Evolution for Enabling Virtual Field Trials," *IEEE Trans. Antennas Propag.*, vol. 62, no. 6, pp. 3242–3256, 2014.
- [25] J. Tropp, "Greed is Good: Algorithmic Results for Sparse Approximation," *IEEE Trans. Inf. Theory*, vol. 50, no. 10, pp. 2231–2242, 2004.